J. Plasma Physics (2010), *vol.* 76, *parts* 3&4, *pp.* 501–511. © Cambridge University Press 2010
doi:10.1017/S0022377809990663

Levitated dust particles subjected to plasma jet

C. M. TICOŞ, I. JEPU, C. P. LUNGU
P. CHIRU, V. ZAROSCHI and A. M. LUNGU
National Institute for Lasers, Plasma and Radiation Physics, 077125 Bucharest, Romania
(cata_ticos@yahoo.com)

(Received 30 November 2009 and accepted 7 December 2009, first published online 15 January 2010)

Abstract. A dust crystal levitated in the sheath of a radio-frequency plasma is subjected to a pulsed plasma jet expelled from a minicoaxial gun. The dust particles, initially found at rest and self-organized in a 3-D structure, are dragged by the plasma jet for a short distance and come to rest when the action of the jet terminates. The trajectories of the microparticles are tracked in vertical and horizontal planes with a high-speed camera. From *in situ* observations of dust particle dynamics the dust acceleration is compared to numerical simulations.

1. Introduction

Plasma crystals are amazing self-organized 3-D structures relatively easy to create in low ionized plasmas, with dimensions of a few millimeters. The regular arrangement of dust particles in plasma crystals resembles that of atoms in crystals. Thus, some properties of crystalline matter can be studied at much more convenient space and time scales in analogy with the dynamics of dust particles [1]. A typical experimental setup in which plasma crystals can be produced includes two parallel-plate electrodes spaced by a few centimeters, one grounded and the other driven by a high-voltage radio-frequency (RF) signal. Although formation of plasma crystals is also possible in DC plasmas or Q-machines, it appears that low-power RF plasmas are the preferred type of discharge, which can provide the right conditions for obtaining stable and large plasma crystals [2]. The recipe is simple. Dust particles of a few microns in size are let to fall through the plasma to accumulate charges on their surface. As they come close to an horizontal electrode immersed in plasma they settle into its sheath and float as long as the discharge is powered. Here the electric force is proportional with their charge and the sheath electric field. The electric force compensates for the force of gravity by pointing upwards. There are other forces acting on the dust particles, such as the drag exerted by the ions flowing to the electrode, by the neutral atoms, or by gas convection due to the temperature gradients, but in most experimental conditions these are negligible in comparison to the electrical and gravity forces [3].

One of the main features of plasma crystals is the strong electrostatic coupling between the particles. This is possible as the Debye length is much larger than the interparticle distance a_d: $\lambda_D \gg a_d$. The interaction potential between the dust particles is mediated by the factor $\exp(-a_d/\lambda_D)$. It is expected that an increase in the plasma density by keeping the other plasma parameters constant would

https://doi.org/10.1017/S0022377809990663 Published online by Cambridge University Press

lead to a weakening of the dust–dust interaction. This effect would lead to visible modifications in the structure of the plasma crystal.

In this paper we subject a strongly coupled dust cloud initially formed in a low-ionized RF plasma to a denser plasma flow created in a coaxial gun. We present first observations of a dust crystal dragged by the plasma jet. The dust dynamics is discussed based on the recorded high-speed images.

Interaction of dust particles with plasma or ion flows is a topic of wide interest. It spans a diversity of experimental situations, in which dust crystals with a high number of layers are crossed by flowing ions accelerated by the sheath electric field in a RF plasma [4], clouds of dust particles are exposed to ions drifting in DC plasmas [5], hot-filament discharges [6], to plasmas produced in Q-machines [7], or to dense plasma flows [8, 9]. Simulations were carried out for describing at a microscopic level the plasma flow-dust interaction by using particle-in-cell (PIC) codes [10, 11] and for validating established theoretical models [12, 13]. The paper is organized as follows: In Sec. 2 of the paper we present the experimental setup and the electrical circuit for generating the plasma discharge. The plasma parameters as well as the dynamics of the dust particles are discussed in Sec. 3 and followed by conclusions.

2. Experiment

It is well known that one important feature which characterizes the physics of dust particles in low-ionized gases is the strength of electrostatic coupling. This situation is best described by the coupling parameter Γ defined as the ratio of Coulomb potential energy to dust kinetic energy. For strongly coupled plasma crystals Γ is larger than 100. In dense plasmas it is well below 1; in principle no crystals can form and none have been observed so far.

If somehow it would be possible to vary one of the dusty plasma parameters, e.g. to increase the electron density, any changes in the dust–dust electrostatic coupling should be in principle observed. Of course, one extremely important issue in this scenario has to do with the correlation between the rate of change of the plasma density and the charging time of a dust particle.

High-speed imaging is a powerful diagnostic tool in dusty plasmas. While dust trajectories are easy to track in a low-ionized gas, monitoring of the particles' dynamics is much more challenging in denser plasmas. There are two important features which characterizes these two cases: First, the flux of ions impinging on a dust grain can accelerate it to high speed and move it out of the viewing plane, and secondly, the dense plasma can be quite luminous and its emissivity can hinder dust detection. In the first case it is always a difficult task to be able to maintain the focus on the microscopic dust, especially for fast-moving grains, while the problem revealed in the second case can be partially solved by introducing in the imaging optics chain a transmission filter tuned for the laser line used to illuminate the particles. In dense and rapid dusty plasma jets, image capturing is even more restrictive and limited to time-windows of only tens of microseconds as the particles leave rapidly the viewing region. Luckily, there are situations when dust illumination is not needed and dust emissivity is intensified due to interaction with the plasma. This is typical for fusion plasmas, where observation of glowing particles can last from a few milliseconds to several seconds. Finally, there are situations when the use of high-speed cameras is not possible and dust detection

https://doi.org/10.1017/S0022377809990663 Published online by Cambridge University Press

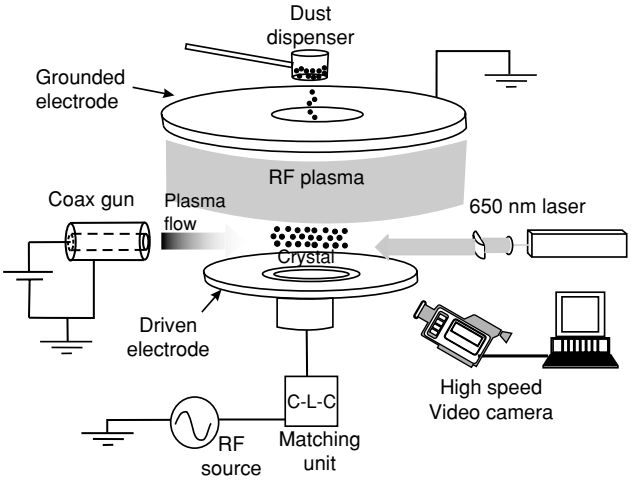


Figure 1. Experimental setup including the coaxial plasma gun.

is realized indirectly from collisions with surfaces [14]. The dustspeed and angle of the trajectory are then deduced by analyzing the size and appearance of the crater produced at the impact or by measuring the stopping distance of the particle in soft materials such as aerogel.

The imaging system of the experiment presented here combines high-speed capture and zoom in capabilities in order to track the dust particles moderately accelerated by a plasma jet. At the same time, there are two simultaneous discharges in the vacuum chamber: the RF discharge, which creates a quite tenuous plasma, and the plasma jet, which is denser, much brighter and much more opaque. Experiments in which ionization of the gas is induced simultaneously from different sources are not new, one example being the DC-biased pixel of a grided electrode, which produced a bright spot inside an RF plasma [15].

2.1. Plasma crystal in RF discharge

An RF discharge produced in argon between two parallel-plate electrodes serves as the background plasma for producing the dust crystal, as shown in Fig. 1. Monodispersive melamine formaldehyde (MF) ($\rho = 1.51$ g cm^{-3}) microparticles with a diameter $2r_d = 6.07$ μm are released from a cup through a hole in the grounded electrode. The particles fall through the plasma and settle into the sheath of the RF-driven electrode. Here they self-arrange into a 3-D crystal with an average intergrain distance of $a_d = 300$–600 μm.

The plasma is excited by a signal with a peak-to-peak (p–p) amplitude of 120 V delivered from an RF power generator AG 0013. An automated C-L-C-type matching network model ATN 5 is tuned to optimize the transfer of power to the plasma, which can attain a maximum value of 100 W. The reflected power in the system is low, by carefully tuning of the matching network, and is below 5 %.

A vacuum system consisting of a forevacuum and turbomolecular pumps (Leybold D4B and 151, respectively) evacuate the air from the chamber down to 10^{-5} Torr after which argon is introduced through a needle valve until the desired pressure is reached. A Penningvac PTR90 is used to monitor the pressure.

https://doi.org/10.1017/S0022377809990663 Published online by Cambridge University Press

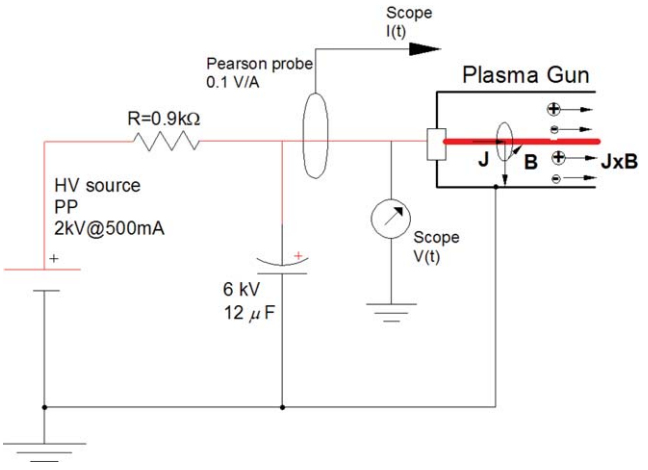


Figure 2. (Color online) Electrical circuit of the coaxial plasma gun.

For dust imaging, a high-speed camera Photron FastCam PCI 1024 with an acquisition rate of up to 109 500 fps (with full resolution 1024×1024 pixels up to 1000 fps, while at maximum speed only 126×16 pixels) is used to record the dust trajectories. The camera is provided with a macro lens Nikon 60 mm f/2.8 D AF, a set of spacing rings with 8, 12 and 36 mm and a tele-converter 2×. A laser sheath obtained by passing a 25-mW laser beam from a laser diode with emission at 650 nm through a cylindrical length with $f = 10$ cm is used to illuminate the dust particles.

2.2. Plasma coaxial gun

A plasma jet is produced in a miniature coaxial plasma gun. Its design is based on a larger and more powerful coaxial plasma gun, which has been successfully used in accelerating dust particles to hypervelocites [16]. The gun comprises a center rod with a diameter $\phi = 12$ mm made of brass and a stainless steel coaxial cylinder with an inner diameter of 25 mm. The length of the coaxial gap is 55 mm. The electrodes of the gun are coupled to a DC power supply, which can deliver up to 2 kV at 0.5 A. The electrical circuit is shown in Fig. 2. A capacitor bank with $C = 12$ μF is charged from the power supply through a power resistor $R = 900$ Ω. The coaxial gun is positioned at 10 to 50 mm from the confining ring sitting on the RF electrode, such that the bottom of the coaxial electrode grazes the surface of the electrode.

The output voltage of the power supply is raised up to the threshold given by the Paschen law (≈ 600 V for our configuration) and the gas becomes ionized. The ionization inside the coaxial gun is eased in the presence of the RF plasma. A pulsed current is generated in the circuit while the voltage on the electrodes of the gun drops and the capacitor bank gets discharged. The current density increases and generates an azimuthal magnetic field inside the coaxial gap. Here the $\mathbf{J} \times \mathbf{B}$ force acting on the charged particles of the ionized gas are pushed toward the nozzle of the gun. Plasma flow speeds of the order of km s^{-1} can be obtained.

Current and voltage probes (Pearson and Tektronix, respectively) are used to record the electrical parameters of the discharge produced in the coaxial gun. Their variation in time during a pulse is presented in Fig. 3. While in practice a continuous

https://doi.org/10.1017/S0022377809990663 Published online by Cambridge University Press

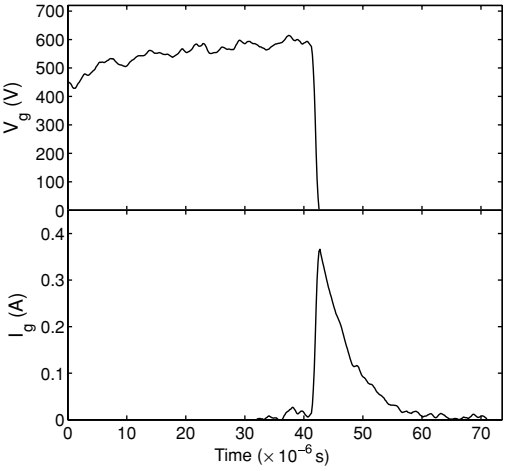


Figure 3. Voltage (V_g) and discharge current (I_g) in the coaxial gun during a plasma pulse.

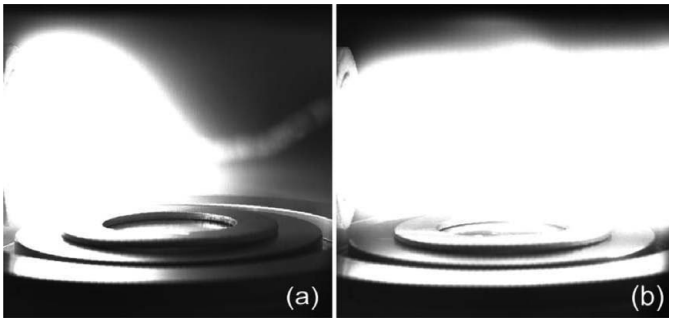


Figure 4. Launch of plasma jet from coaxial gun within the space filled by the RF discharge where the plasma crystal is formed.

operation of the gun can be easily achieved by raising the output voltage of the power supply well beyond the discharge threshold, here we are interested in the action of a single pulse on the crystal. In this regime, the capacitor charges up in $\tau_c \approx RC = 10$ μs and releases its energy on the electrodes in a single pulse. The jet goes through the whole space between the parallel plates. The two pictures in Fig. 4 were acquired at 125 fps with a shutter speed of 8 ms. From our observations we deduce a lower limit for the jet speed of at least 1 km s^{-1}.

3. Results

In Fig. 5(a) a stable plasma crystal is levitated in the sheath of the RF-driven electrode, in argon at 275 mtorr. The transfer of the RF power to the plasma is fairly good, with a forward value of 7 W and reflected power of 2 W. The gas pressure is relatively close to the 'melting' point of the crystal, which is about 240 mtorr. It is chosen to ensure the formation of a higher sheath which allows for more convenient imaging of the dust particles floating above the driven electrode.

https://doi.org/10.1017/S0022377809990663 Published online by Cambridge University Press

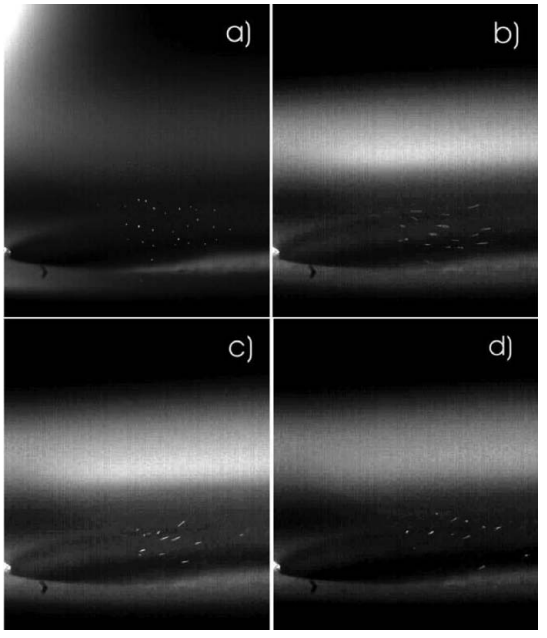


Figure 5. Stable plasma crystal and jet approaching from left at t = 0 (a); plasma-dragged microparticles t = 8 ms (b); ascending trajectories of dust particles t = 16 ms (c) and slowing down and eventual stop of the dust particles t = 24 ms (d).

A consequence is that the particles are more spread with larger intergrain spacing in the vertical plane illuminated with the laser beam.

The coaxial gun is fired and the jet approaches the dust crystal from the left in Fig. 5(a). The dust particles are put in motion pushed by the plasma jet in the horizontal direction (Fig. 5b). Some of the particles have an ascending trajectory, at an angle which varies between 5° and 45° Fig. 5(c). The speed of the dust particles is in the range of 1 to 10 cm s^{-1}. It is important here to mention that the electric force is always present in the z direction, i.e. perpendicular on the RF electrodes, as the RF plasma is on and the particles are situated in the plasma sheath. The resultant force acting on the dust particles is the contribution of electric, gravity and plasma drag forces. In the pictures, the jet is visible in the upper left corner of (a) while the RF plasma and the darker sheath can be better seen in the intensified images in (b), (c) and (d).

There could be at least two reasons for the observed dust trajectories. In many observations the jet expelled from the coaxial gun was not always horizontal. Its direction of propagation was seen to be self-deflected toward the upper, grounded electrode of the RF discharge. This phenomenon is unpredictable in the sense that shots with parallel flow are followed randomly by shots with inclined flow. For our presented data in Figs 5(a)–(d) the camera was focused on the dust crystal and set for an acquisition speed (125 fps), which was optimal for dust tracking. The jet could not be seen simultaneously with the dust particles and its propagation time was too fast for the camera capabilities, well below the frame rate. Other phenomena that could contribute to dust propelling up in the sheath is the perturbation of the sheath and the change in the electric field distribution, which can affect the

https://doi.org/10.1017/S0022377809990663 Published online by Cambridge University Press

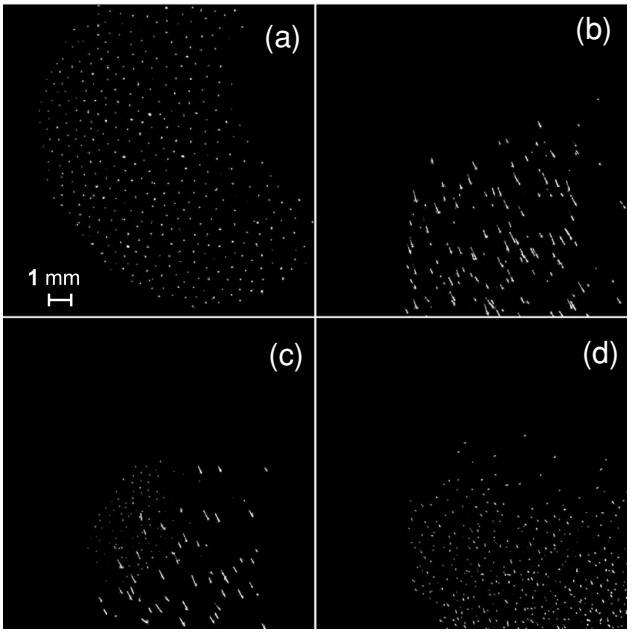


Figure 6. Top view of plasma crystal during a shot: initial stable plasma crystal (a); plasma-dragged microparticles (b); mixed stationary and moving microparticles (c); selforganization into a crystal (d).

balance of forces acting on the grains. A higher density of ions at the edge of the RF plasma can in fact intensify the electric field in the sheath and can also increase the magnitude of the upward electric force. The shape of the dust trajectory resembles a parabola: the microparticles first go upwards and fall back into the sheath after the jet has left the region (Fig. 5d).

The effect of the plasma jet on dust crystal dynamics is also observed by real-time monitoring of the crystal from the top. The focused laser beam is illuminating a narrow horizontal section positioned approximately at the middle of the crystal. In Fig. 6 a sequence of four pictures shows the response of the crystal to the jet from the coaxial gun. The pictures are processed with dedicated software in order to increase their contrast, brightness and intensity. The power fed into the RF discharge is 6 W and the gas pressure is 410 mtorr. The stable crystal is presented in Fig. 6(a). Here one can see large, bright dots, which constitute the dust layer under observation but also smaller dots corresponding to dust particles from an adjacent dust layer. Thus, one can distinguish the clear sight of one crystal layer and the weaker appearance of dust particles from the next layer seen in the background. After the jet is fired we first observe the dust particles moving in the direction of the plasma flow. The displacement of the crystal boundary is about 7.4 mm (Fig. 6b). The speed of the dust particles is again inferred from the length of their visible traces divided by the exposure time. The recorded traces range from 0.02 to 0.65 mm in a time period of 8 ms. The velocity of the microparticles is about 0.2 to 8 cm s^{-1}. The crystal seems to keep its structure, with all the microparticles moving in the same direction.

https://doi.org/10.1017/S0022377809990663 Published online by Cambridge University Press

Frame (b) is acquired at 32 ms from the moment of firing, while frame (c) is taken at 40 ms. In frame (c) some of the dust particles are still moving while many are at rest. We believe that these apparently static particles come to rest in a shorter time due to different drag forces exerted by the flow. The ion flow from the jet might not be perfectly uniform and have density gradients in its cross section. On this image there is a mix of moving and static dust particles, which do not seem to interact with each other. The image is, however, a visual effect associated with the position of the camera which records only a projection of the 3-D phenomena. The viewed dust particles are spaced from each other but in the vertical direction and belong to different horizontal layers. This supposition is sustained by the observations of dust motion in a vertical plane: some particles move while others are at rest, as seen in Fig. 5(d). In Fig. 6(d) taken at 144 ms from time zero, the dust particles regroup themselves and move in the opposite direction of the flow, again forming a crystal. The sheath is regaining its initial, unperturbed shape and the dust particles fill up slowly, in a few hundreds of milliseconds, the space above the confining ring.

An interesting observation is that right after the jet is fired, for several frames the dust particles are out of the horizontal laser plane and are not observed by the camera. This could be an effect of the jet propagation within the inter-electrode space. When the jet is deflected toward the upper electrode, and propagates at an angle, the horizontal dust layers are probably displaced vertically. Also, during firing the sheath is perturbed and, therefore, some of the dust particles can be pushed out of the field of view of the fast camera. These issues will be systematically investigated in future work.

Another important observation is that the dust particles are still bunched together and overall the dust cloud does not lose its confinement. The plasma jet pulse is very brief, but much longer than the dust-charging time. In principle the charge on the dust particles is quickly adjusted by the flow of new ions and electrons coming from the coaxial gun. Considering the long observation time of the camera, there would be enough time for the repulsive force to act on the dust particles and produce visible changes in the arrangement of the particles. The dust–dust coupling seems not to be affected and the inter-grain coupling does not suffer visible modifications. One conclusion is that transport of a dust crystal within the sheath of an RF plasma is possible.

The motion of the dust particles shown in the recorded images synchronized with the plasma jet ignition is the clear evidence that the plasma wind is pushing the dust particles and the ion drag plays an important role in dust dynamics. In fact, it can be shown using a simple model that the force exerted by ions can indeed accelerate the micron-size dust particles to speeds of the order of a few mm s^{-1}. Here we consider a plasma pulse of 10 μs, with an electron temperature of 2 eV ions at room temperature ($T_i = 0.025$ K) and a density of 10^{16} m^{-3}. We also suppose that ions have only an axial motion in the direction of the $\mathbf{J} \times \mathbf{B}$ force, which accelerates them to $v_P = 10$ to 20 km s^{-1}. These assumptions of cold ions and higher plasma density than of a typical RF plasma are acceptable considering the energy and power injected into the discharge (≈ 2 J) during a short pulse. In our experiment the density and temperature of the RF plasma have not been measured. Since our electrode configuration is very similar to that of [17], it can be assumed that our setup produces an RF plasma with parameters in the same range, i.e. $T_e \approx 2$ to 3.5 eV, and $n_e \approx 1$ to 3×10^{15} m^{-3}.

https://doi.org/10.1017/S0022377809990663 Published online by Cambridge University Press

Table 1. Simulated dust-charging time τ_c, potential U_d, terminal speed v_d and plasma drag accelerations (F_{col}, F_{Coul}) obtained for two sets of plasma flow parameters, i.e. density n_e and flow speed v_P.

n_e (m^{-3})	v_P (km s^{-1})	τ_c (μs)	U_d (V)	v_d (mm s^{-1})	F_{col}/m_d (m s^{-2})	F_{Coul}/m_d (m s^{-2})
10^{16}	10	1.1×10^{-2}	−12.83	0.21	0.61	3.04×10^{-3}
10^{17}	20	5.6×10^{-4}	−11.79	5.01	8.66	4.02×10^{-5}

In the simplest description of dust charging, the orbital motion-limited (OML) framework, the electrons follow a Boltzmann distribution and ions are collected from an area larger than the cross section πr_d^2 of the spherical dust [18]:

$$b_c = r_d \sqrt{1 - \frac{2eU_d}{m_i v_i^2}}, \tag{3.1}$$

where $U_d < 0$ is the dust potential and v_i is the mean speed of ions, which is a combination of the plasma flow speed and the ion thermal speed, $v_i = \sqrt{8k_B T_i/\pi m_i + v_P^2}$ [19]. We neglect here collision of ions with the neutral gas atoms. The dust particles are charged by the plasma jet hitting the dust surface:

$$I_i = en_e v_i \pi b_c^2, \quad \text{and} \quad I_e = en_e \pi r_d^2 \sqrt{\frac{8k_B T_e}{\pi m_e}} \exp\left(-\frac{eU_d}{k_B T_e}\right). \tag{3.2}$$

The charging time can be expressed as $\tau_c = [T_e/T_i + (v_{Te}/v_i)\exp(-y_0)]/\alpha_n$, where $\alpha_n = n_e e^2 r_d v_i/(\sqrt{2\pi}\varepsilon_0 k_B T_e)$ and $y_0 = -eU_d/k_B T_e$ [3].

In the limit of short-range scattering of ions on the dust particle [13], the contributions of direct collisions (F_{col}) and Coulombic interaction (F_{Coul}) add up their effect and result in a plasma wind force given by [3]

$$F_{id} = \pi r^2 m_i n_i v_{Ti} v_i \left(1 - \frac{2eU_d}{m_i {v_P}^2}\right) + \frac{2\pi r^2 n_{is} (eU_d)^2}{m_i {v_P}^2} ln\Lambda, \tag{3.3}$$

where

$$\Lambda = \left(\frac{{\lambda_D}^2 + {b_0}^2}{{b_c}^2 + {b_0}^2}\right) \text{and } b_0 = \frac{eV_d}{m_i {v_P}^2.} \tag{3.4}$$

The dust-charging time τ_c for the parameters of the plasma jet is well below the duration of the plasma jet, as shown in Table 1. The charge on the dust particle submerged by the pulsed plasma flow can adjust quickly to the new ion and electron currents and a new equilibrium value is established. In the plasma jet the dust acceleration due to the Coulomb force of ions is small compared to the direct drag exerted by colliding ions with the dust surface. However, the total plasma drag force is strong enough to cause the dust particle to reach speeds in agreement with our measurements. Also, the fact that dust particles are put in motion by the plasma jet is a clear indication of the more intense ion drag than that manifested by the ion flow in the RF sheath.

4. Conclusions

A dust crystal made of monodispersive MF particles and formed in the sheath of an argon RF plasma was subjected to the action of a plasma jet obtained from

https://doi.org/10.1017/S0022377809990663 Published online by Cambridge University Press

a miniature coaxial gun. The particles are put in motion by the plasma jet while they are still levitated in the sheath. Their trajectories are tracked by a high-speed camera. The ion drag force is pushing the dust particles in the direction of the jet although some features in the dust dynamics, such as the ascending trajectory inside the sheath, remain unclear. The plasma pulse has a duration much longer than the dust-charging time. The crystal is still confined and no change in the dust–dust coupling is observed, which could possibly be induced by a modification in the plasma screening length.

Acknowledgements

This work was supported in part by the Romanian National University Research Council (CNCSIS-UEFISCSU) under contract RP-10, within the PNCDI2 program.

References

[1] Shukla, P. K. and Eliasson, B. 2009 Colloquium: fundamentals of dust-plasma interactions. *Rev. Mod. Phys.* **81**, 25–44.

[2] Morfill, G. E. and Thomas, H. 1996 Plasma crystals. *J. Vac. Sci. Technol.* A**14**, 490–495.

[3] Shukla, P. K. and Mamun, A. A. 2002 Dynamics of dust grains. In: *Introduction to Dusty Plasma Physics*. Bristol, UK: Institute of Physics pp. 70–93.

[4] Liao, C.-T., Teng, L.-W., Tsai, C.-Y., Io, C.-W. and I, L. 2008 Lagrangian-eulerian micromotion and wave heating in nonlinear self-excited dust-acoustic waves. *Phys. Rev. Lett.* **100**, 185004–1/4.

[5] Ratynskaia, S. et al. 2004 Experimental determination of dust-particle charge in a discharge plasma at elevated pressures. *Phys. Rev. Lett.* **93**, 085001–1/4.

[6] Hirt, M., Block, D. and Piel, A. 2004 Measurement of the ion drag force on free falling microspheres in a plasma. *Phys. Plasmas* **11**, 5690–5696.

[7] Barkan, A., Merlino, R. L. and D'Angelo, N. 1995 Laboratory observation of the dust acoustic wave mode. *Phys. Plasmas* **2**, 3563–3565.

[8] Wang, Z. H., Ticos, C. M. and Wurden, G. A. 2007 Dust trajectories and diagnostic applications beyond strongly coupled dusty plasmas. *Phys. Plasmas* **14**, 103701–1/11.

[9] Ticos, C. M., Wang, Z. H., Wurden, G. A., Kline, J. L. and Montgomery, D. S. 2008 Plasma jet acceleration of dust particles to hyper velocities. *Phys. Plasmas* **15**, 103701–1/9.

[10] Hutchinson, I. H. 2005 Ion collection by a sphere in a flowing plasma: 3. Floating potential and drag force I H. *Plasma Phys. Contr. Fusion* **47**, 71–87.

[11] Lapenta, G. 2002 Nature of the force field in plasma wakes. *Phys. Rev.* E **66**, 026409–1/6.

[12] Kilgore, M. D., Daugherty, J. E., Porteous, R. K. and Graves, D. B. 1993 Ion drag on an isolated particulate in low-pressure discharge. *J. Appl. Phys.* **73**, 7195.

[13] Khrapak, S. A., Ivlev, A. V. and Morfill, G. E. 2004 Momentum transfer in complex plasmas. *Phys. Rev.* E **70**, 056405–1/9.

[14] Castaldo, C. et al. 2007 Diagnostics of fast dust particles in tokamak edge plasmas. *Nucl. Fusion* **47**, L5–L9.

[15] Annaratone, B. M., Antonova, T., Goldbeck, D. D., Thomas, H. M. and Morfill, G. E. 2004 Complex-plasma manipulation by radio frequency biasing. *Plasma Phys. Control. Fusion* **46** B495–B509.

https://doi.org/10.1017/S0022377809990663 Published online by Cambridge University Press

[16] Ticos, C. M., Wang, Z. H., Dorf, L. A. and Wurden, G. A. 2006 Plasmadynamic hyper velocity dust injector for the national spherical torus experiment. *Rev. Sci. Instrum.* **77**, 10E304–1/3.

[17] Ticos, C. M., Dyson, A. and Smith, P. W. 2004 The charge on falling dust particles in a RF plasma with DC negative bias. *Plasma Sources Sci. Technol.* **13**, 395–402.

[18] Allen, J. E. 1992 Probe theory – the orbital motion approach. *Phys. Scripta* **45**, 497–503.

[19] Barnes, M. S., Keller, J. H., Forster, J. C., O'Neill, J. A. and Coultas, D. K. 1992 Transport of dust particles in glow discharge plasmas. *Phys. Rev. Lett.* **68**, 313–316.

https://doi.org/10.1017/S0022377809990663 Published online by Cambridge University Press